INTERNATIONAL JOURNAL FOR NUMERICAL METHODS IN FLUIDS, VOL. 15, 355–372 (1992)

PREDICTION OF TURBULENT OFFSET JET FLOWS WITH AN ASSESSMENT OF QUICKER SCHEME

HYEONG-MO KOO* AND SEUNG O. PARK

Department of Aerospace Engineering, Korea Advanced Institute of Science and Technology, 373-1 Kusong-Dong, Yusung-Ku, Taejon, Korea

SUMMARY

The QUICKER scheme extended for non-uniform rectangular grid systems has been applied to predict the turbulent offset jet flows. Computational results obtained with the QUICKER scheme are compared with those from the skew-upwind and the hybrid schemes. Computational results include the reattachment length, the velocity profile, the axial velocity decay curve, and the shear stress distribution. In the sense of an overall agreement with the experimental data, the QUICKER scheme is found to be superior to the other two schemes. Boundary conditions are carefully set up to account for various flow conditions. Special attention has been given to the set-up of entrainment boundary condition. It is emphasized that the numerical diffusion due to streamline-to-grid skewness far exceeds the turbulent diffusion in offset jet flows; therefore, a numerical scheme that would minimize the numerical diffusion is a prerequisite for a better prediction of the turbulent offset jet flows.

KEY WORDS Turbulent offset jet flow Hybrid differencing Skew-upwind differencing QUICKER differencing Numerical diffusion Entrainment boundary condition

INTRODUCTION

Offset jet is a typical flow that can be found in many engineering applications, such as in environment dischargers, heat exchangers, fluid injector systems and combustion chambers. In an offset jet flow, a jet is discharged parallel to and offset from a solid wall with or without a secondary free stream. The flow is characterized by the longitudinal variation of streamline curvature, skewed impingement onto a flat surface, a recirculating region, and the development into a wall jet flow (Figure 1). When a numerical prediction of the flow is attempted, characteristic features of each component contributing to the complex flow structure must be properly taken into account. A recent numerical calculation of an offset jet flow performed by Yoon *et al.*[1] showed that the numerical scheme had a more pronounced effect on the accuracy of the solution than the turbulence model. Even though the flow far downstream becomes a wall jet type, the recirculating region just downstream of the jet exit requires an elliptic type solution procedure. Further, the streamline curvature in offset jet flows is in general severer than in the rearward-facing step flows. Therefore, it is expected that the numerical diffusion error due to streamline-to-grid skewness will be significant in the prediction of offset jet flows.

* Present address: Consumer Electronics Business R&D Centre, Samsung Electronic Company, Metan-Dong, Kwonsun-ku, Suwon, Korea.

0271–2091/92/150355–18$14.00

Received September 1990
Revised January 1992

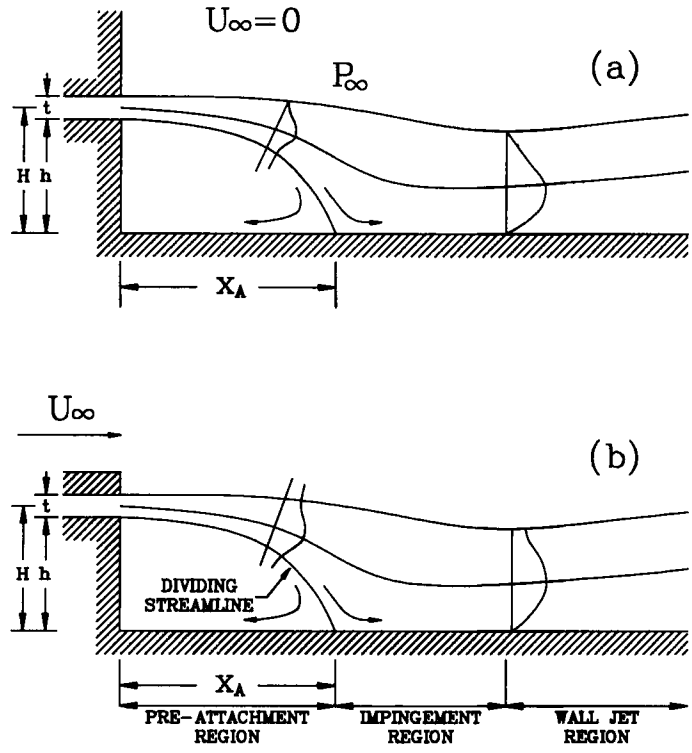

Figure 1. Offset jet flow configurations: (a) Pelfrey and Liburdy;[6] (b) Hoch and Jiji[7]

An evaluation of the various discretization schemes concerning numerical diffusion based on the computation of turbulent, annular and twin parallel jets was carried out by Leschziner and Rodi.[2] Patel and Markatos[3] reported the results of their work, where the merits and drawbacks of eight discretization schemes were investigated in the context of the computation of laminar flows of a sudden expansion pipe and a lid-driven cavity. One of the conclusions was that the more accurate schemes were not of general applicability while the more general schemes might be too inaccurate. In a more general framework, the issues regarding the approximation of the convection term were discussed in the review article of Leschziner;[4] numerous references on the subject can be found therein.

Despite its wide variety of engineering applications, efforts to numerically predict turbulent offset jet flows have been rare. For an accurate prediction of an offset jet flow, the problem of numerical diffusion associated with a strong streamline curvature has to be brought into attention. No previous work other than Reference 1 seems to have touched upon the issue of numerical diffusion in predicting turbulent offset jet flows. In this work, we attempted to investigate the effect of several discretization schemes for the convection term on the prediction of mean flow field of turbulent offset jet flows. Thus, it became necessary not to allow turbulence model variations in order to avoid ambiguity in interpreting the predicted results. The turbulence model adopted in this study was the standard k–ε model as given by Launder and Spalding.[5] The offset jet flows experimentally studied by Pelfrey and Liburdy[6] and by Hoch and Jiji[7] were computed and the computational results were compared with the available experimental data. Based on the comparison, the performance of the hybrid, the skew-upwind, and the QUICKER

schemes was evaluated. The QUICKER scheme adopted in this study is an extended version[9] of the original QUICKER[8] to non-uniform rectangular grid systems.

MATHEMATICAL FORMULATION

Governing equations

The governing equations for two-dimensional, incompressible, steady turbulent flows can be written in a rectangular Cartesian co-ordinate system as follows, with the turbulent stresses substituted by eddy viscosity relations:

continuity equation

$$\frac{\partial U}{\partial x}+\frac{\partial V}{\partial y}=0. \tag{1}$$

momentum equations

$$\frac{\partial}{\partial x}(\rho U^2)+\frac{\partial}{\partial y}(\rho UV)=-\frac{\partial P}{\partial x}+\frac{\partial}{\partial x}\left(\mu_{\text{eff}}\frac{\partial U}{\partial x}\right)+\frac{\partial}{\partial y}\left(\mu_{\text{eff}}\frac{\partial U}{\partial y}\right)+S_U, \tag{2}$$

$$\frac{\partial}{\partial x}(\rho UV)+\frac{\partial}{\partial y}(\rho V^2)=-\frac{\partial P}{\partial y}+\frac{\partial}{\partial x}\left(\mu_{\text{eff}}\frac{\partial V}{\partial x}\right)+\frac{\partial}{\partial y}\left(\mu_{\text{eff}}\frac{\partial V}{\partial y}\right)+S_V, \tag{3}$$

where U and V are the velocities in the horizontal (x) and the normal (y) directions, respectively, ρ is the density and P the pressure. S_U and S_V are the appropriate source terms. The effective viscosity, μ_{eff}, is given by the combination,

$$\mu_{\text{eff}}=\mu+\mu_t, \tag{4}$$

where μ and μ_t are the laminar and the turbulent viscosities, respectively.

Turbulence model

The standard k–ε model employed in this study adopts the eddy viscosity concept and determines the eddy viscosity from the values of the time-averaged turbulence kinetic energy, k, and its dissipation rate, ε, according to

$$\mu_t=C_\mu\rho\frac{k^2}{\varepsilon}. \tag{5}$$

The distributions of k and ε are determined from the solution of the following semi-empirical transport equations:

$$\rho U\frac{\partial k}{\partial x}+\rho V\frac{\partial k}{\partial y}=\frac{\partial}{\partial x}\left(\frac{\mu_{\text{eff}}}{\sigma_k}\frac{\partial k}{\partial x}\right)+\frac{\partial}{\partial y}\left(\frac{\mu_{\text{eff}}}{\sigma_k}\frac{\partial k}{\partial y}\right)+G-\rho\varepsilon, \tag{6}$$

$$\rho U\frac{\partial \varepsilon}{\partial x}+\rho V\frac{\partial \varepsilon}{\partial y}=\frac{\partial}{\partial x}\left(\frac{\mu_{\text{eff}}}{\sigma_\varepsilon}\frac{\partial \varepsilon}{\partial x}\right)+\frac{\partial}{\partial y}\left(\frac{\mu_{\text{eff}}}{\sigma_\varepsilon}\frac{\partial \varepsilon}{\partial y}\right)+C_{\varepsilon 1}\frac{\varepsilon}{k}G-C_{\varepsilon 2}\rho\frac{\varepsilon^2}{k}, \tag{7}$$

where

$$G\equiv\mu_{\text{eff}}\left\{2\left[\left(\frac{\partial U}{\partial x}\right)^2+\left(\frac{\partial V}{\partial y}\right)^2\right]+\left(\frac{\partial U}{\partial y}+\frac{\partial V}{\partial x}\right)^2\right\}.$$

The coefficients in the equations (5)–(7) take the following values, as given by Launder and Spalding:[5] $C_\mu = 0{\cdot}09$; $C_{\varepsilon 1} = 1{\cdot}44$; $C_{\varepsilon 2} = 1{\cdot}92$; $\sigma_k = 1{\cdot}0$; $\sigma_\varepsilon = 1{\cdot}3$.

As mentioned earlier, no modification of the turbulence model was attempted to draw a definite conclusion about the discretization schemes. The method of wall function as boundary conditions near the solid surface was adopted. The use of wall function for recirculating or impinging flows is, in fact, questionable. However, the wall function approach is normally taken for practical purposes, owing partly to the fact that a reliable approach to cope with separating or reattaching flows is not yet established. In the present computation, a two-layer approach where the inner layer is represented by the viscous sublayer ($y^+ < 11{\cdot}63$) and the inertial sublayer ($y^+ > 11{\cdot}63$) was adopted as was originally implemented in TEACHT. The y^+ values of the first grid points from the wall for the various cases of the present computation ranged from 20 to 50.

NUMERICAL PROCEDURE

General remarks

The two momentum equations (2) and (3) and equations (6) and (7) describing the transport of k and ε may be expressed in the following form:

$$\frac{\partial}{\partial x}(\rho U\phi)+\frac{\partial}{\partial y}(\rho V\phi)=\frac{\partial}{\partial x}\left(\Gamma_\phi \frac{\partial \phi}{\partial x}\right)+\frac{\partial}{\partial y}\left(\Gamma_\phi \frac{\partial \phi}{\partial y}\right)+S_\phi, \tag{8}$$

where ϕ represents any dependent variable of interest. Γ_ϕ is the appropriate diffusivity coefficient for the variable ϕ. The source term, S_ϕ, includes the pressure gradient terms for the momentum equations and encompasses the generation and the decay rate of the dependent variables for the transport equations for the turbulence quantities. A staggered grid system is used where the control volumes for U and V are centred on the faces of the control volumes for the scalar variables, ρ, k and ε; the pressure nodes are located at the centre of the continuity control volume, which is known to suppress the wiggles or the checkboard patterns of the pressure.[10]

Equation (8) is converted into its finite difference equivalent by integrating it over a control volume surrounding each node. For a typical grid node shown in Figure 2, a finite volume

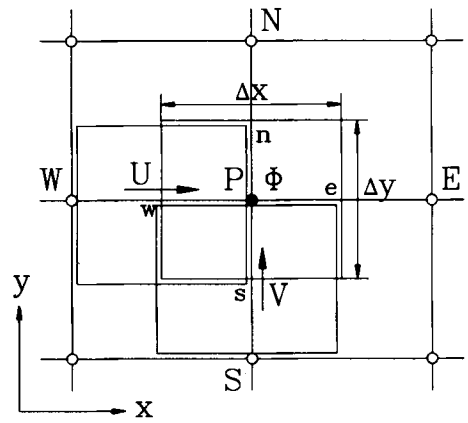

Figure 2. Staggered grid system and control volume for each dependent variable

approximation to equation (8) can be expressed as

$$\left\{\rho U\phi-\Gamma_\phi\frac{\partial\phi}{\partial x}\right\}_e A_e^\phi+\left\{\rho U\phi-\Gamma_\phi\frac{\partial\phi}{\partial x}\right\}_w A_w^\phi+\left\{\rho V\phi-\Gamma_\phi\frac{\partial\phi}{\partial y}\right\}_n A_n^\phi$$
$$+\left\{\rho V\phi-\Gamma_\phi\frac{\partial\phi}{\partial y}\right\}_s A_s^\phi=S_\phi \mathrm{CV}_P^\phi, \tag{9}$$

where the A's denote the areas of the cell faces in the four compass point directions (n, s, e, w) located midway between the grid nodes, and CV is the control volume surrounding the point P.

Discretization schemes

To express equation (9) in terms of the ϕ values on the grid points surrounding the node of interest, the ϕ profiles between any two grid points must be assumed in an appropriate manner. As usual, the second-order-accurate central difference approximation is used to represent the diffusion terms. It is the convection term that is of interest, in that its treatment can lead to the generation of troublesome false diffusion, which can have damaging effects on the solution accuracy, especially when the streamwise grid Peclet number is large. Particularly, for flows of the type having large longitudinal curvature like the offset jet, it is indispensable to first minimize this numerical diffusion for accuracy of the solution. Simply refining the grid could make it possible to use the non-diffusive central differencing by reducing the mesh Peclet number, which is obviously an expensive way in terms of computer time and storage limitations. An attractive way to overcome this problem is to use more complex and sophisticated discretization methods for convection terms. As is well known, the false diffusion is generated from two sources: (1) the introduction of a truncation error, which arises when the second-order-accurate central differencing method to approximate the convective transport is replaced by the first-order-accurate upwind differencing scheme to assure stability; (2) the skewness between the grid lines and the direction of the flow velocity. Especially, the false diffusion arising from the streamline-to-grid skewness may drastically impair the accuracy of the computation.[11] In this study, three different differencing methods were used to approximate the convection terms: the hybrid scheme, the skew-upwind scheme and the QUICK scheme. The hybrid scheme, proposed by Patankar,[10] uses the first-order upwind difference when the grid Peclet number is greater than 2, and adopts the central differencing otherwise. The skew-upwind differencing scheme, proposed by Raithby,[12] considers the direction of the velocity vector and assumes a locally linear ϕ profile in the cross-stream direction while estimating the fluxes by convection in order to reduce numerical diffusion. The QUICK (quadratic upstream interpolation for convection kinematics) scheme, originally proposed by Leonard,[13] assumes a locally parabolic polynomial distribution of ϕ across the control volume surface at three consecutive nodal positions, two of which are located on either side of the surface in question and the third one on the upstream. However, the original QUICK formulation occasionally makes the influence coefficients of the finite difference equations negative, which often causes instability, as is often the case when the central differencing technique is employed. This is especially true when the curvature correction terms are treated as sources and the flow rates are relatively high. Pollard and Siu[8] proposed revised formulations of the QUICK scheme to improve the stability property, which were referred to as the QUICK extended form (QUICKE) and the QUICK extended and revised form (QUICKER). Both formulations guaranteed the positiveness of the influence coefficients in the finite difference equations, and were presented only for a uniform grid system in their work. Therefore, in the present study, we adopted the QUICKER formulation which was modified for a non-uniform rectangular grid system in our previous work.[9]

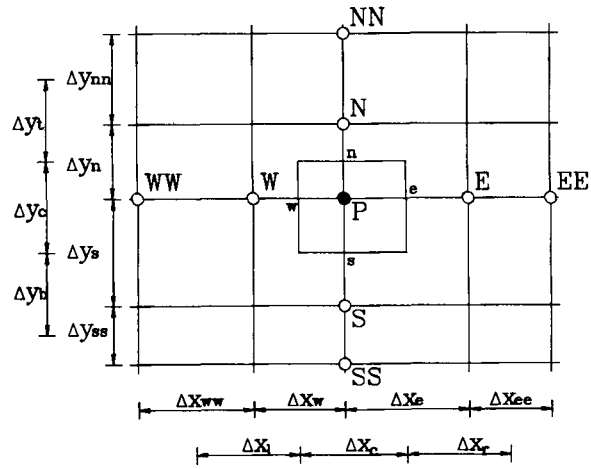

Figure 3. Nine-point configuration and length definitions of a non-uniform rectangular grid system

The QUICKER scheme modified for a non-uniform rectangular mesh is briefly discussed below. The value of a convected variable on the east cell face, ϕ_e, is expressed as follows using the neighbouring values shown in Figure 3:

$$\phi_e=\frac{1}{2}(\phi_E+\phi_P)-\frac{\Delta x_e^2}{8}(\mathrm{CURVN_e})+\frac{\Delta y_e^2}{24}(\mathrm{CURVT_e}) \tag{10}$$

where

$$\mathrm{CURVN_e}=\mathrm{CURVN(P)}, \quad \mathrm{CURVT_e}=\mathrm{CURVT(P)} \quad \text{if } U_e\geq 0,$$
$$\mathrm{CURVN_e}=\mathrm{CURVN(E)}, \quad \mathrm{CURVT_e}=\mathrm{CURVT(E)} \quad \text{if } U_e<0.$$

CURVN and CURVT represent the normal and the transverse curvatures of the ϕ profile about the e surface. The detailed expression for these can be obtained in Reference 14. The transverse curvature effect is usually neglected for simplicity and convenience, with minor loss of accuracy. In this study, therefore, we also neglected the transverse curvature effect. The ϕ values on the rest of the cell faces can be obtained similarly. However, the original QUICK formulation occasionally causes the influence coefficients to be negative in the finite difference equations, which may lead to instability. This is especially true when the curvature correction terms are treated as sources and the flow rates are relatively high. Integration of equation (9), with the ϕ profiles given as equation (10), results in the following finite difference form:

$$\phi_P=\frac{B_E^\phi\phi_E+B_W^\phi\phi_W+B_N^\phi\phi_N+B_S^\phi\phi_S+S_a^\phi}{B_P^\phi-S_b^\phi}, \tag{11}$$

where the B's are the influence coefficients made up of the contributions from diffusion and convection, and S's are the source terms containing all the terms resulting from transforming the partial differential equations into their finite difference equivalents but not explicitly contained in equation (11).

When the idea of Pollard and Siu[8] (that the fractional influence coefficients be always positive) is applied to a non-uniform rectangular grid system shown in Figure 3, the following expressions

are obtained: (These expressions can easily be shown to be identical to those of Pollard and Siu when the grid spacing is uniform.)

$$B_E = M_e^+ \left\{ D_e + \left(\frac{1}{2} + \frac{\Delta x_e}{4\Delta x_{ee}} \right) C_e \right\} + M_e^- \left\{ D_e - \left(\frac{1}{2} + \frac{\Delta x_e}{4\Delta x_{ee}} \right) C_e \right\} - M_w^- \frac{\Delta x_w^2}{\Delta x_c \Delta x_e} \frac{C_w}{8},$$

$$B_W = M_w^+ \left\{ D_w + \left(\frac{1}{2} + \frac{\Delta x_w}{4\Delta x_{ww}} \right) C_w \right\} + M_w^- \left\{ D_w - \left(\frac{1}{2} + \frac{\Delta x_w}{4\Delta x_{ww}} \right) C_w \right\} + M_e^+ \frac{\Delta x_e^2}{\Delta x_c \Delta x_w} \frac{C_e}{8},$$

$$B_N = M_n^+ \left\{ D_n + \left(\frac{1}{2} + \frac{\Delta y_n}{4\Delta y_{nn}} \right) C_n \right\} + M_n^- \left\{ D_n - \left(\frac{1}{2} + \frac{\Delta y_n}{4\Delta y_{nn}} \right) C_n \right\} - M_s^- \frac{\Delta y_s^2}{\Delta y_c \Delta y_n} \frac{C_s}{8},$$

$$B_S = M_s^+ \left\{ D_s + \left(\frac{1}{2} + \frac{\Delta y_s}{4\Delta y_{ss}} \right) C_s \right\} + M_s^- \left\{ D_s - \left(\frac{1}{2} + \frac{\Delta y_s}{4\Delta y_{ss}} \right) C_s \right\} + M_n^+ \frac{\Delta y_n^2}{\Delta y_c \Delta y_s} \frac{C_n}{8},$$

$$B_P = B_E + B_W + B_N + B_S,$$

where

$$M_i^+ = \frac{C_i + |C_i|}{2C_i}, \qquad M_i^- = \frac{C_i - |C_i|}{2C_i}, \quad i = \text{e, w, n, s} \tag{12a}$$

and the C_i's represent the flow rates across the ith cell face and $D_e = \Gamma_\phi A_e / \delta x_e$, etc. The above expressions for the influence coefficients treat the flow direction only by the M_i's, so that inconsistency and ambiguity at the boundary cells can be removed. The source terms are given as

$$\begin{aligned} S_a^{\phi'} = S^\phi &+ \frac{1}{8} \left\{ M_e^- \frac{\Delta x_e^2}{\Delta x_r \Delta x_{ee}} C_e \phi_{EE} - M_w^+ \frac{\Delta x_w^2}{\Delta x_l \Delta x_{ww}} C_w \phi_{WW} \right\} \\ &+ \frac{1}{8} \left\{ M_n^- \frac{\Delta y_n^2}{\Delta y_t \Delta y_{nn}} C_n \phi_{NN} - M_s^+ \frac{\Delta y_s^2}{\Delta y_b \Delta y_{ss}} C_s \phi_{SS} \right\} \\ &- M_e^+ \left\{ 1 + \frac{\Delta x_e}{8} \left(\frac{2}{\Delta x_{ee}} - \frac{1}{\Delta x_c} \right) \right\} C_e \phi_E + M_w^- \left\{ 1 + \frac{\Delta x_w}{8} \left(\frac{2}{\Delta x_{ww}} - \frac{1}{\Delta x_c} \right) \right\} C_w \phi_W \\ &- M_n^+ \left\{ 1 + \frac{\Delta y_n}{8} \left(\frac{2}{\Delta y_{nn}} - \frac{1}{\Delta y_c} \right) \right\} C_n \phi_N + M_s^- \left\{ 1 + \frac{\Delta y_s}{8} \left(\frac{2}{\Delta y_{ss}} - \frac{1}{\Delta y_c} \right) \right\} C_s \phi_S \end{aligned}$$

and

$$\begin{aligned} S_b^{\phi'} = &M_e^+ \frac{\Delta x_e}{4} \left(\frac{1}{\Delta x_{ee}} - \frac{1}{\Delta x_w} \right) C_e - M_e^- \left\{ 1 + \frac{\Delta x_e}{8} \left(\frac{2}{\Delta x_{ee}} - \frac{1}{\Delta x_r} \right) \right\} C_e \\ &+ M_w^+ \left\{ 1 + \frac{\Delta x_w}{8} \left(\frac{2}{\Delta x_{ww}} - \frac{1}{\Delta x_l} \right) \right\} C_w - M_w^- \frac{\Delta x_w}{4} \left(\frac{1}{\Delta x_{ww}} - \frac{1}{\Delta x_e} \right) C_w \\ &+ M_n^+ \frac{\Delta y_n}{4} \left(\frac{1}{\Delta y_{nn}} - \frac{1}{\Delta y_s} \right) C_n - M_n^- \left\{ 1 + \frac{\Delta y_n}{8} \left(\frac{2}{\Delta y_{nn}} - \frac{1}{\Delta y_t} \right) \right\} C_n \\ &+ M_s^+ \left\{ 1 + \frac{\Delta y_s}{8} \left(\frac{2}{\Delta y_{ss}} - \frac{1}{\Delta y_b} \right) \right\} C_s - M_s^- \frac{\Delta y_s}{4} \left(\frac{1}{\Delta y_{ss}} - \frac{1}{\Delta y_n} \right) C_s \\ &- \frac{1}{8} \left\{ M_w^- \frac{\Delta x_w^2}{\Delta x_c \Delta x_e} C_w - M_e^+ \frac{\Delta x_e^2}{\Delta x_c \Delta x_w} C_e + M_s^- \frac{\Delta y_s^2}{\Delta y_c \Delta y_n} C_s - M_n^+ \frac{\Delta y_n^2}{\Delta y_c \Delta y_s} C_n \right\}. \end{aligned} \tag{12b}$$

Though somewhat complicated, a closer investigation of equation (12a) will show that the influence coefficients are always positive. In the QUICKER formulation, the linearized source term is lumped into a completely explicit form, so that

$$S_a^\phi = S_a^{\phi'} + S_b^{\phi'} \phi_P^* \tag{13a}$$

and

$$S_b^\phi = 0, \tag{13b}$$

where ϕ_P^* is the current ('in-store') value of ϕ_P. This type of explicit treatment may result in a longer computation time to obtain a converged solution. However, the undesirable stability problem when S_b^ϕ is positive is always avoided.

It should be mentioned that the skew-upwind and the QUICKER schemes were used only in the two momentum equations in the present study. The transport equations of turbulence quantities, k and ε, were discretized by the hybrid differencing method, as usual, considering the fact that the transport equations for k and ε are source-term dominated, so that values generated for k and ε would be virtually immune to the effects of false diffusion.[2]

Code validation

The coefficients given in equations (12a) and (12b) are somewhat complex and, thus, the implementation of these relations into a code is prone to coding errors. As a way to ensure that the code used in the present work is free from coding errors, we first computed the Blasius boundary layer flow. The computation was performed on a 60×40 (streamwise $\times$ normal) uniform mesh system. The predicted velocity profile at $Re_x = 400$ is shown in Figure 4. The good agreement between the predicted profile and the Blasius solution suggests that the present code works properly.

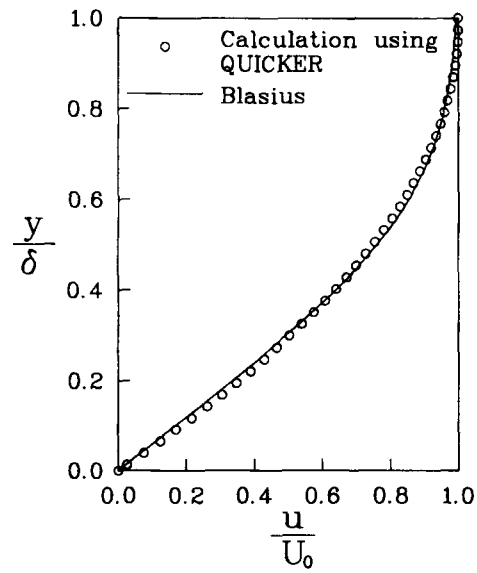

Figure 4. Predicted velocity profile of the Blasius flow

Boundary conditions

The flow configuration of interest in this study is depicted in Figure 1. The jet flow is exhausted from a nozzle of width t into the surroundings, which impinges upon the bottom plate through a curved path, generating a recirculating region, and develops into a wall jet flow. When the Reynolds number based on the nozzle width is very large (generally, greater than 10^4), it is known that the impingement distance is determined by the offset ratio. The cases computed in this study were the two types. The first case was the flow shown in Figure 1(a), where the jet issues into a stagnant surroundings and the boundary above the nozzle exit is blocked by a solid wall. The same flow configuration was experimentally studied by Pelfrey and Liburdy[6] (designated as PL hereinafter). The second case was the one shown in Figure 1(b), where the jet issues in a co-flowing outer stream. In this flow configuration, the solid wall above the nozzle exit is absent. Therefore, the upstream entrainment property is very different from the first case. This case was experimentally studied by Hoch and Jiji[7] (designated as HJ hereinafter). In order to predict these two distinct types of flow, care must be exercised in implementing the boundary conditions. For the first case, the Neumann boundary conditions of vanishing gradients of the dependent variables across both the upper entrainment and the downstream outflow boundary were imposed. When the boundary conditions were imposed in this manner, the continuity constraint became redundant for the control volume at the uppermost right corner located at the intersection of the two abutting boundaries. Unless this double imposition of continuity constraint is removed, the TDMA (tri-diagonal matrix algorithm) would fail along either of the lines and a point-iterative solver would fail at this control volume.[15] To overcome this problem, the level of pressure at this control volume, which may serve as a reference pressure, must be specified: the value of the pressure correction in Reference 15 was set to be zero during the solution process and, hence, the continuity constraint became inactive. For the second case, the specification of upstream boundary condition differs depending upon whether the surrounding fluid is stagnant or is co-flowing with a finite speed. When the surrounding fluid is stagnant, the Neumann boundary condition of vanishing gradients of U and V across the upstream entrainment and the downstream outflow boundary is a plausible approximation. From the continuity constraint, this amounts to specifying zero V velocity on both the upstream and the downstream boundary. Specification of the pressure level of the upper right corner as explained above removes the redundancy of the continuity constraint. The same treatment for the upper left corner, however, is not desirable since the pressure level can hardly be specified for two different locations. To

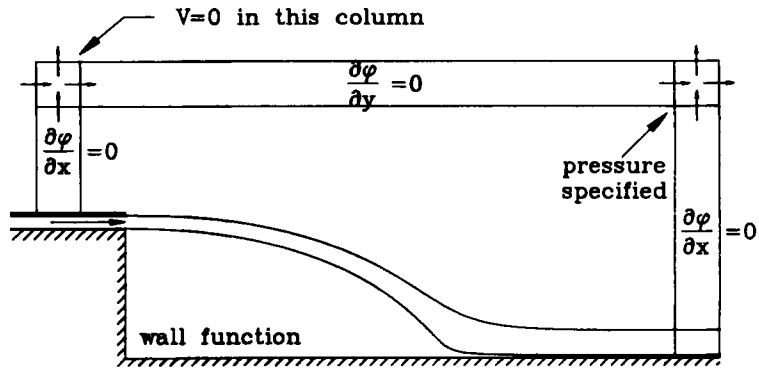

Figure 5. Boundary conditions for the offset jet flow field

remedy this situation, the V velocity component was set to be zero along the upstream entrainment boundary, and the V momentum equation was solved from the next line of that edge. This removed the other continuity redundancy at the upstream boundary and converged solutions were obtained. Specification of boundary conditions for this case is illustrated in Figure 5. When the surrounding fluid is not stagnant and the velocity profile from the experimental data is available, the redundancy problem discussed above does not occur. In this case the boundary treatment similar to that for Pelfrey's experiment was sufficient for the solution procedure.

The velocity profiles at the jet exit for the two cases were taken as uniform. The k and ε values at the jet exit were assumed to be uniform, which later proved to have negligible influence on the downstream development of the flow. On the lower plate and near the upstream plug walls, the standard log-law-based wall function for smooth wall was used for the parallel velocity component and the turbulence quantities k and ε.

Computational details

The solutions to equation (11) were obtained by adopting the SIMPLE algorithm employed in the general two-dimensional computer code TEACHT.[16] The major modifications incorporated in the code included the set-up of influence coefficients to account for various discretization schemes. In this study, iterations were continued until the residual for each equation was less than 0.5×10^{-3}.

The offset jet flow of PL had an offset ratio, H/t, of 7 and the nozzle Reynolds number of 15 000. Among the various cases of HJ experiment, computation was mainly devoted to the case of the nozzle Reynolds number of 15 000 with the nozzle thickness of 1·17 cm. The downstream and the top boundary of the computational domain were located at a distance of 75 and 35 times the jet nozzle width, respectively. The downstream distance roughly corresponded to 4–7·5 times the (experimental) reattachment length and the top boundary distance to 4–11·7 times the offset height. For the case of HJ flow, the upstream entrainment boundary was located at a distance of one offset height from the plane of the jet exit. Most of the computational results reported in this work were from the computation carried out using a mesh made of 75×60 non-uniformly distributed grid lines, unless otherwise noted. A typical grid system used in the present work is shown in Figure 6. In the regions near the wall boundary and along the axis of the jet nozzle, finer grids were used to resolve steep changes of the flow variables. The leftmost portion of the grid system in front of the vertical wall was used for the flows of HJ and was made inactive for the PL case. The results of grid refinement study will be discussed later.

COMPUTATIONAL RESULTS AND DISCUSSIONS

As has been mentioned earlier, the offset jet flows dealt with in this study can be classified by the presence of free stream and the upstream wall. The overall flow picture will change according to these conditions. Streamline patterns for the PL and HJ flows are shown in Figures 7(a) and 7(b), respectively. Due to the difference in the upstream entrainment boundary, the entrained flow patterns differ considerably from each other. For the same offset ratio, the reattachment length of the PL case was found to be shorter than that of the HJ case. The shorter reattachment length of the PL case may be attributable to the vertically entrained flow. The reattachment length, x_A, obtained from the experimental data of PL was about 13 times the nozzle width. The calculated values of x_A using the three differencing schemes (hybrid, skew-upwind and QUICKER schemes) were 10·8, 14·2 and 13·8 times the nozzle width, respectively. The reattachment point from the

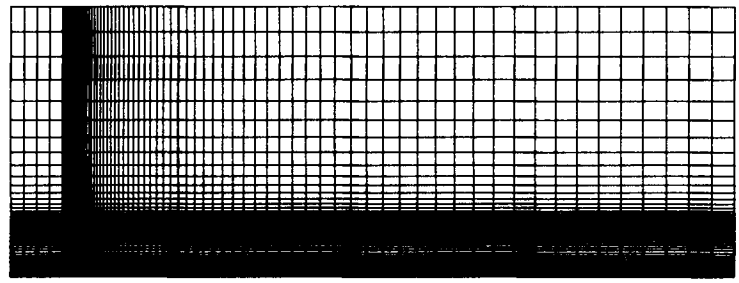

Figure 6. Typical grid system employed in the present computation

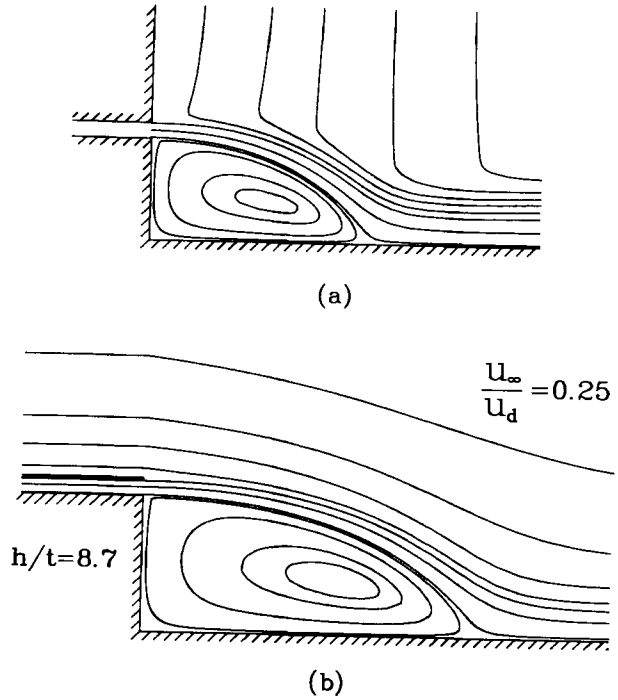

Figure 7. Streamline patterns of the offset jet flows: (a) Pelfrey and Liburdy;[6] (b) Hoch and Jiji[7]

computational data was defined to be the point where the wall shear stress on the bottom plate vanishes, and was estimated by linear interpolation. The reattachment lengths determined either from the experimental data or from the numerical calculation were about 2 times the nozzle offset height, H. The reattachment length of the offset jet flow is, thus, much shorter than that of the rearward-facing step flows, which is generally known to be about 7 times the step height. The streamline curvature in offset jet flows is, therefore, much larger than in the rearward-facing step flows. The reattachment length variations with the change of offset ratio for various free stream conditions as experimented by HJ and the corresponding computational data are illustrated in Figure 8. It is seen that the predictions of the QUICKER and the skew-upwind differencing schemes are generally in better agreement with the experimental data than those of the hybrid

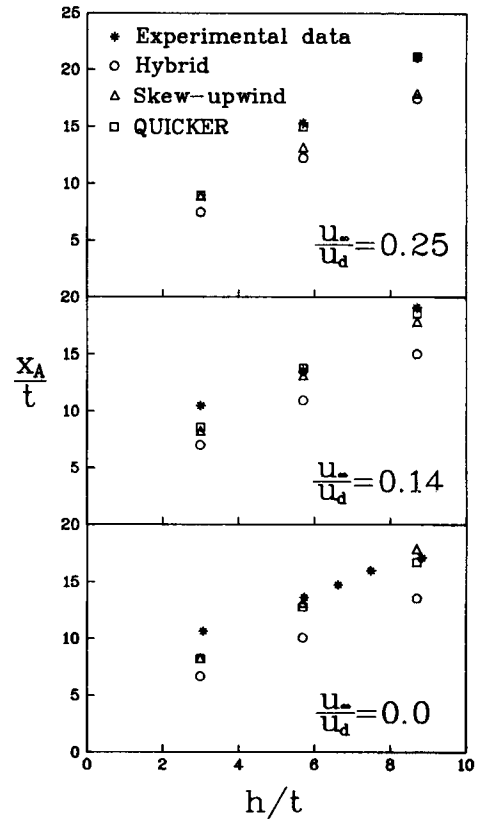

Figure 8. Variation of the reattachment length with offset jet height (Experimental data from Hoch and Jiji[7])

scheme. It is interesting to note that the performance of the skew-upwind differencing scheme deteriorates when the velocity of the external stream becomes large. The QUICKER scheme performs much better than the skew-upwind scheme in this case.

Figure 9 displays the maximum axial velocity variations of the jet along the offset-jet–wall-jet trajectory for various offset heights in an HJ flow. As the jet impinges on the bottom wall, the pressure of the jet increases. Consequently, the axial velocity decays rapidly. After the reattachment, the high pressure causes the (attached) wall jet to accelerate. As the pressure relaxes to the ambient pressure, the maximum axial velocity of the wall jet starts to decay. This qualitative nature of velocity decay was well mimicked by all the three schemes. However, none of the three discretization schemes predicted correctly the maximum axial velocity and its development. The hybrid scheme resulted in a faster decay of the maximum velocity just downstream of the jet exit, so that the position of the local minimum in the maximum velocity distribution curve appeared earlier. The local minimum value was predicted rather poorly by the skew-upwind scheme. The performance of the QUICKER scheme also was no better than the other two.

Figure 10 shows the profiles of the x-component velocity in the pre-attachment and the impingement regions for the case of PL. The predicted profiles clearly demonstrate that the skew-upwind and the QUICKER schemes are superior to the hybrid scheme. Perhaps, the use of the hybrid scheme should be discouraged. The hybrid scheme is so diffusive that the momentum of

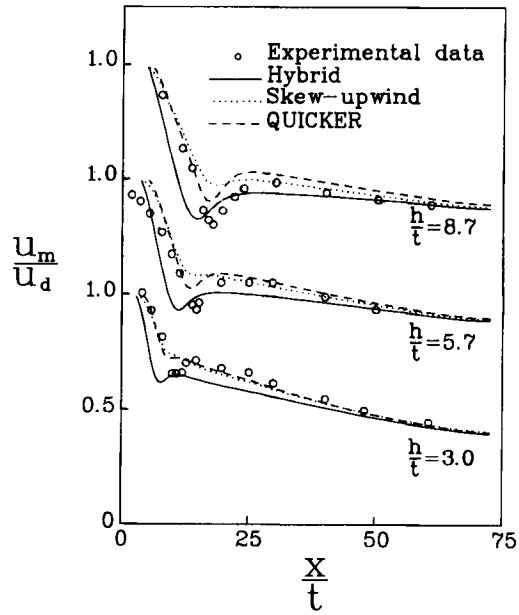

Figure 9. Maximum axial velocity decay for an offset jet flow (Experimental data from Hoch and Jiji[7])

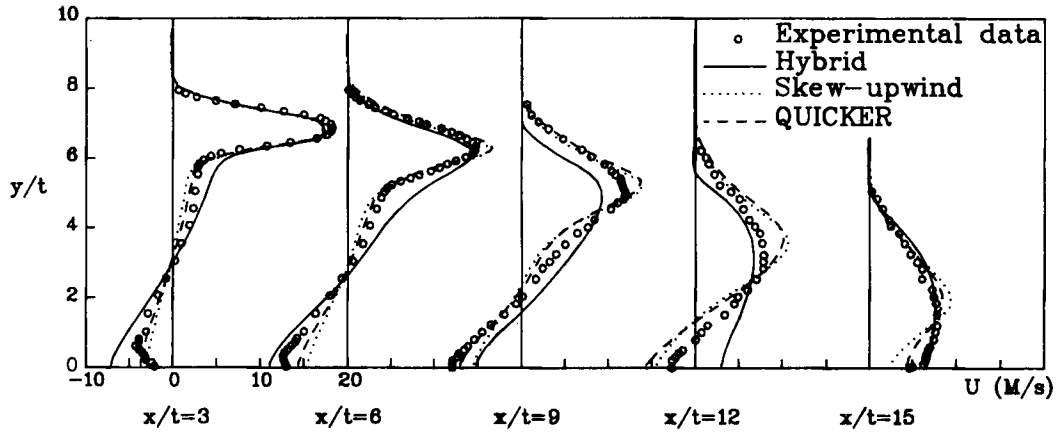

Figure 10. Streamline velocity profiles (Experimental data from Pelfrey and Liburdy[6])

the jet is transported into the recirculating region, resulting in a faster decay of the maximum velocity (Figure 9) and a shorter reattachment length (Figure 8). Grid dependency tests carried out for the QUICKER and the hybrid schemes revealed the following interesting result. In Figures 11 and 12, the streamwise velocity profiles at $x/t=6$ computed with various grid arrangements are compared with one another. The QUICKER scheme virtually produced grid-independent velocity profiles. The velocity profiles predicted with the hybrid scheme, as seen in Figure 12, change continually with the grid system. It is seen that the velocity profile moves very slowly towards the profile obtained using the QUICKER scheme. It may be conjectured that a

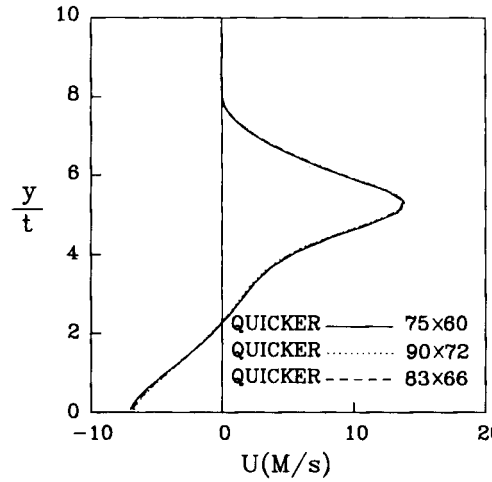

Figure 11. Velocity profiles with various grid arrangements (QUICKER scheme)

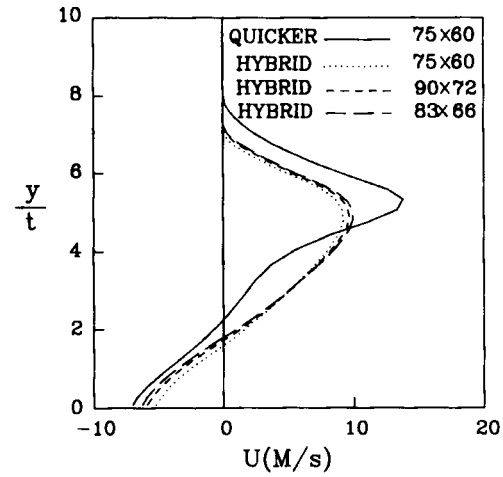

Figure 12. Velocity profiles with various grid arrangements (hybrid scheme)

much finer grid system than those used in the present work is necessary to get a favourable solution.

The wall shear stress variation in the impingement region past the reattachment point is shown in Figure 13. The predicted distributions differ considerably from the measured data. However, we see that the distributions obtained with the QUICKER and the skew-upwind schemes show a closer agreement with the experimental data. The discrepancy is partly due to the adoption of the wall function approach not suitable for reattaching flows. It is conjectured that a more refined near-wall treatment than the present wall function approach may improve the prediction of the shear stress distribution.

The effect of numerical diffusion on the solution can be assessed when we compare the magnitude of the eddy viscosity and the magnitude of the numerical diffusion. The magnitude of

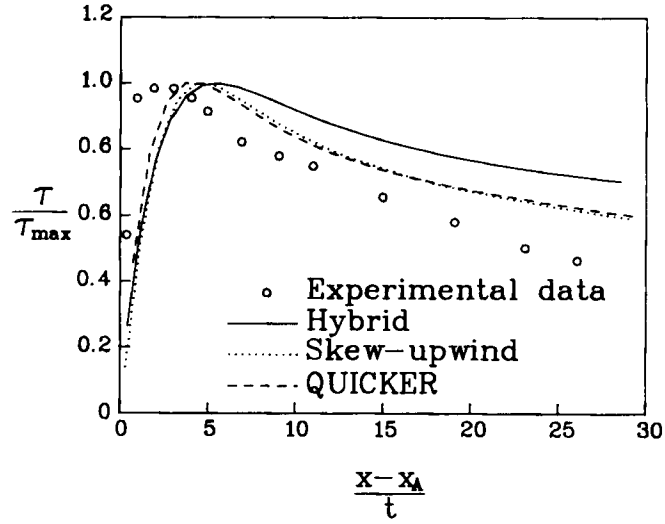

Figure 13. Shear stress distributions past the reattachment point (Experimental data from Pelfrey and Liburdy[6])

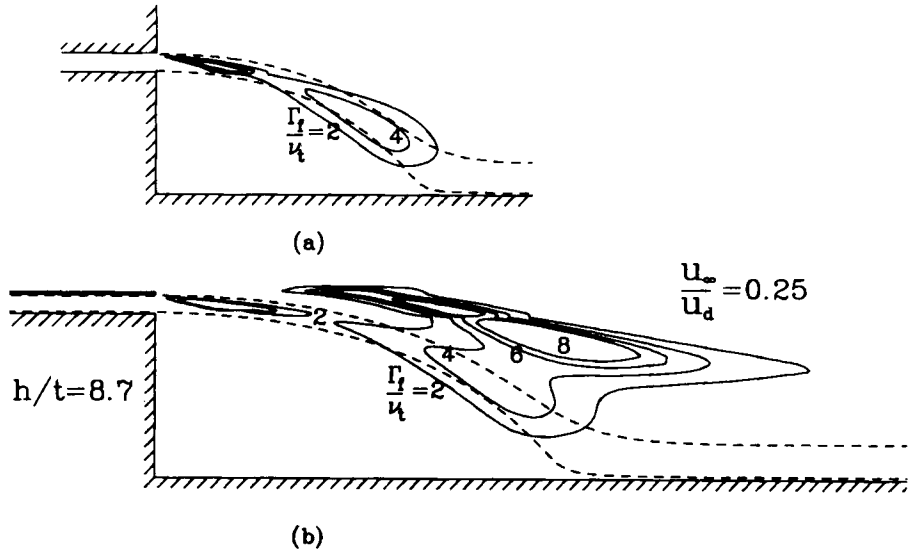

Figure 14. Ratio of numerical diffusivity to turbulent diffusivity: (a) PL flow; (b) HJ flow

the numerical diffusion due to streamline-to-grid skewness associated with the first-order upwind differencing is given by

$$\Gamma_f = \frac{|V|\,\Delta x\,\Delta y \sin 2\theta}{4(\Delta y \sin^3\theta + \Delta x \cos^3\theta)}, \tag{14}$$

where θ is the skewness angle, and Γ_f represents the numerical (artificial or false) diffusion coefficient.[17] The ratio of the numerical diffusivity, Γ_f, to the eddy viscosity, ν_t, as obtained by

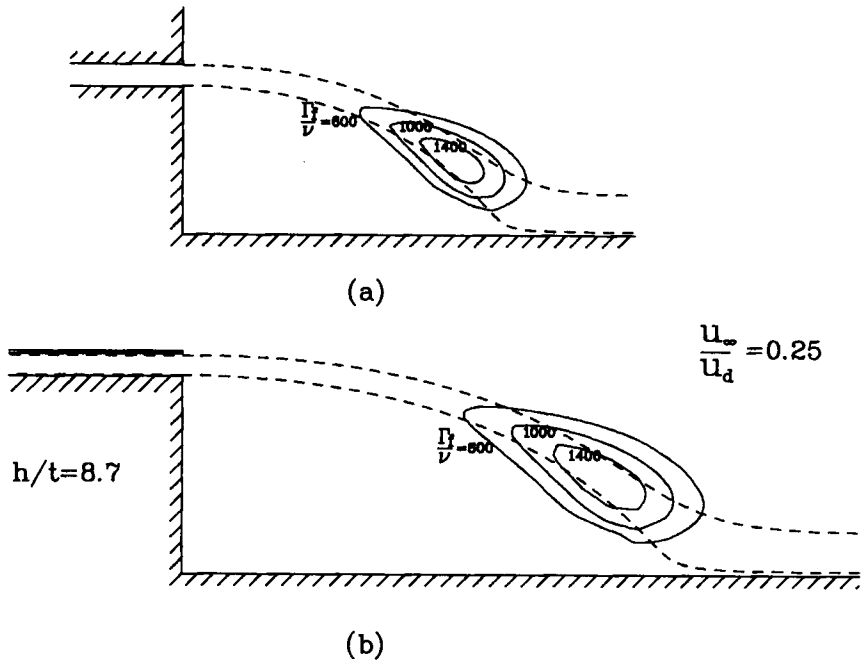

Figure 15. Ratio of numerical diffusivity to laminar diffusivity: (a) PL flow; (b) HJ flow

using the standard k–ε model is sketched in Figure 14. For reference purposes, the contours of the ratio of the turbulent viscosity to the laminar viscosity are shown in Figure 15. The dashed lines in both figures represent the jet streamlines. The value of Γ_f was computed using equation (14) based on the velocity field given by the QUICKER solution. Thus, the distribution of Γ_f shown is not real but is sufficient for qualitative assessment. Figure 14 clearly demonstrates that the numerical diffusivity overwhelms the eddy viscosity in the region of curved shear layer. Rather poor predictions of the reattachment length, the maximum velocity decay, and the velocity profiles using the hybrid scheme might have been caused by the large numerical diffusion. Since the eddy viscosity was computed based on the k–ε model, the ratio of the numerical diffusion to the turbulent diffusion would be somewhat different from that seen in Figure 14 if a higher-order turbulence model were employed. However, it is not likely that the magnitude of the turbulent viscosity (or its equivalent) predicted with a higher-order model will be far off from that obtained with the standard k–ε model. Thus, we expect that the significance of large numerical diffusion seen in the present flow will more or less remain the same for the cases of turbulence model variations.

CONCLUDING REMARKS

Numerical calculations were carried out for the offset jet flows under various external and geometric conditions using the hybrid, the skew-upwind and the QUICKER schemes. Proper boundary conditions to account for the various flow conditions were set up. It has been shown that the flows of this type could not be accurately predicted by the hybrid scheme commonly employed in engineering practice. Of the three discretization schemes, the QUICKER scheme proved to give the best results. The skew-upwind scheme performed as good as the QUICKER scheme when the velocity of the free co-flowing stream was small. When the free-stream velocity

was large, the skew-upwind scheme performed rather poorly. Because of the severe streamline curvature of offset jet flows, care should be given to properly treat the problem of numerical diffusion. For example, performance test of various turbulence models can be meaningless if the hybrid scheme is used, owing to the overwhelming magnitude of the numerical diffusion, unless a very fine grid system is adopted.

ACKNOWLEDGEMENTS

A part of this research has been supported by the Korea Science and Engineering Foundation under grant number 90-02-00-05.

APPENDIX: NOMENCLATURE

A	area of the cell face
B	influence coefficient in the finite difference equations
C_i	flow rate crossing the ith cell face
$C_\mu, C_{\varepsilon 1}, C_{\varepsilon 2}$	constants in the turbulence model
D_i	diffusion constant across the ith cell face
H	offset distance from the bottom plate to the nozzle centre line
h	offset distance from the bottom plate to the lower nozzle edge
k	turbulent kinetic energy
M_i^+, M_i^-	flags for the direction of C_i
P	static pressure
S_U	source term in the x-direction momentum equation
S_V	source term in the y-direction momentum equation
S_ϕ	source term in the transport equation of ϕ
t	nozzle width
U, V	mean velocity in x- and y-direction, respectively
U_d	discharge velocity of the jet
U_m	maximum velocity along the jet axis
X_A	reattachment length
x, y	horizontal and normal co-ordinate, respectively
ε	dissipation rate of k
Γ_f	numerical diffusion coefficient
Γ_ϕ	diffusivity coefficient for the transport equation of ϕ
ρ	density
σ_k	turbulent Prandtl number in the k transport equation
σ_ε	turbulent Prandtl number in the ε transport equation
ϕ	general dependent variable
μ, μ_t	laminar and turbulent viscosity, respectively
μ_{eff}	effective viscosity
ν, ν_t	laminar and turbulent kinematic viscosity, respectively
$\Delta x, \Delta y$	grid spacing in x- and y-direction, respectively
θ	skewness angle between streamline and grid line

REFERENCES

1. S. H. Yoon, S. E. Eun and M. K. Chung, 'Numerical study on the two-dimensional stepped walljet', *Trans. Korean Soc. Mech. Eng.*, **12**, 865–875 (1988).

2. M. A. Leschziner and W. Rodi, 'Calculation of annular and twin parallel jets using various discretization schemes and turbulence-model variations', *Trans. ASME, J. Fluids Eng.*, **103,** 352–360 (1981).
3. M. K. Patel and N. C. Markatos, 'An evaluation of eight discretization schemes for two-dimensional convection–diffusion equations', *Int. j. numer. methods fluids*, **6,** 129–154 (1986).
4. M. A. Leschziner, 'Modeling turbulent recirculating flows by finite volume methods—current status and future directions', *Int. J. Heat Fluid Flow*, **10,** 186–202 (1986).
5. B. E. Launder and D. B. Spalding, 'The numerical computation of turbulent flows', *Comput. Methods Appl. Mech. Eng.*, **3,** 269–289 (1974).
6. J. R. R. Pelfrey and J. A. Liburdy, 'Mean flow characteristics of a turbulent offset jet', *Trans. ASME J. Fluids Eng.*, **108,** 82–88 (1986).
7. J. Hoch and L. M. Jiji, 'Two-dimensional turbulent offset jet–boundary interaction', *Trans. ASME, J. Fluids Eng.*, **103,** 154–161 (1981).
8. A. Pollard and A. L. W. Siu, 'The calculation of some laminar flows using various discretization schemes', *Comput. Methods Appl. Mech. Eng.*, **35,** 293–313 (1982).
9. H. M. Koo and S. O. Park, 'Extension and applications of the QUICKER scheme to a nonuniform rectangular grid system', *Commun. Appl. Numer. Methods* (in press).
10. S. V. Patankar, *Numerical Heat Transfer and Fluid Flow*, Hemisphere, Washington, 1980.
11. G. D. Raithby, 'A critical evaluation of upstream differencing applied to problems involving fluid flow', *Comput. Methods Appl. Mech. Eng.*, **9,** 75–103 (1976).
12. G. D. Raithby, 'Skew upstream differencing schemes for problem involving fluid flow', *Comput. Methods Appl. Mech. Eng.*, **9,** 153–164 (1976).
13. B. P. Leonard, 'A stable and accurate convection modelling procedure based on quadratic upstream interpolation', *Comput. Methods Appl. Mech. Eng.*, **19,** 59–98 (1979).
14. B. P. Leonard, 'Elliptic systems: finite-difference method IV', in W. J. Minkowycz, E. M. Sparrow, G. E. Schneider, R. H. Pletcher (eds), *Handbook of Numerical Heat Transfer*, Wiley, New York, 1988, Chap. 9.
15. J. P. Van Doormaal and G. D. Raithby, 'Enhancements of the SIMPLE method for predicting incompressible flows', *Numer. Heat Transfer*, **7,** 147–163 (1984).
16. A. D. Gosman, W. M. Pun, A. K. Runchal, D. B. Spalding and M. Wolfstein, *Heat and Mass Transfer in Recirculating Flows*, 2nd edn, Academic Press, London, 1973.
17. G. de Vahl Davis and G. D. Mallinson, 'An evaluation of upwind and central difference approximations by a study of recirculating flow', *Comput. Fluids*, **4,** 29–43 (1976).